NeuroImage: Clinical 29 (2021) 102566

Contents lists available at ScienceDirect

NeuroImage: Clinical

journal homepage: www.elsevier.com/locate/ynicl

Multiparametric *in vivo* analyses of the brain and spine identify structural and metabolic biomarkers in men with adrenomyeloneuropathy

Isaac M. Adanyeguh [a,1], Xiaofang Lou [a,1], Eavan McGovern [a], Marie-Pierre Luton [a], Magali Barbier [a], Elise Yazbeck [a], Romain Valabregue [a,c], Dinesh Deelchand [b], Pierre-Gilles Henry [b], Fanny Mochel [a,d,e,*]

[a] INSERM U 1127, CNRS UMR 7225, Sorbonne Universités, UPMC Univ Paris 06 UMR S 1127, Institut du Cerveau et de la Moelle épinière, ICM, F-75013 Paris, France
[b] Center for Magnetic Resonance Research (CMRR), University of Minnesota, Minneapolis, MN, United States
[c] Center for NeuroImaging Research (CENIR), Institut du Cerveau et de la Moelle épinière, 75013 Paris, France
[d] AP-HP, Pitié-Salpètrière University Hospital, Department of Genetics, Paris, France
[e] University Pierre and Marie Curie, Neurometabolic Research Group, Paris, France

ARTICLE INFO

Keywords:
Adrenomyeloneuropathy
Spinal cord imaging
Metabolite cycling
Fixel-based analysis
Imaging biomarkers
Spinal cord toolbox

ABSTRACT

Objective: Progressive myelopathy causes severe handicap in men with adrenomyeloneuropathy (AMN), an X-linked disorder due to *ABCD1* pathogenic variants. At present, treatments are symptomatic but disease-modifying therapies are under evaluation. Given the small effect size of clinical scales in AMN, biomarkers with higher effect size are needed. Here we used high-resolution magnetic resonance techniques to identify non-invasive *in vivo* biomarkers of the brain and spine with high effect sizes.

Methods: We performed a multiparametric imaging and spectroscopy study in 23 male patients with AMN (age: 44 ± 11) and 23 male controls (age: 43 ± 11) of similar age and body-mass index. We combined (i) macrostructural analyses of the spine, using cross-sectional area (CSA) and magnetization transfer ratio (MTR), (ii) microstructural analyses of the spine and the brain, using diffusion tensor and the newly developed fixel-based analysis, and (iii) advanced metabolic analyses of the spine using metabolite cycling coupled to a semi-LASER sequences.

Results: Macrostructural alterations (decrease in CSA and MTR) were observed in patients at all spinal cord levels studied (C1-T2 for CSA and C1-C5 for MTR) ($p < 0.001$). Microstructural alterations were observed in the spine and brain on diffusion tensor and fixel-based metrics though the latter showed higher effect sizes. Metabolic alterations were observed in patients as a decreased total *N*-acetylaspartate/*myo*-inositol ratio ($p < 0.001$). Overall, MTR showed the highest effect size.

Conclusion: This cross-sectional study supports the use of multiparametric techniques that elucidate the structural, microstructural and metabolic alterations in AMN. These outcome measures should be tested longitudinally and in clinical trials.

Abbreviations: AD, axial diffusivity; ALD, adrenoleukodystrophy; AMN, adrenomyeloneuropathy; CSA, cross-sectional area; MTR, magnetization transfer ratio; tCho, total choline; tCr, total creatine; tNAA, total *N*-acetylaspartate; *myo*-Ins, *myo*-Inositol; CFE, connectivity-based fixel enhancement; CSF, cerebrospinal fluid; CSD, constrained spherical deconvolution; CST, corticospinal tract; DTI, diffusion tensor imaging; EDSS, expanded disability status scale; FA, fractional anisotropy; FBA, fixel-based analysis; FC, fiber cross-section; FD, fiber density; FDC, fiber density and cross-section; FOD, fiber orientation distribution; FOV, Field of view; GRAPPA, generalized autocalibrating partial parallel acquisition; MPRAGE, magnetization-prepared rapid gradient-echo; MRI, magnetic resonance imaging; MRS, magnetic resonance spectroscopy; OVS, outer volume suppression; RD, radial diffusivity; SARA, scale for the assessment and rating of ataxia; SCA, spinocerebellar ataxias; SNR, signal-to-noise ratio; SSPROM, Severity Scoring system for Progressive Myelopathy; TBSS, tract-based spatial statistics; TE, echo time; TR, repetition time; VAPOR, variable pulse power and optimized relaxation delays; VLCFA, very long chain fatty acids.

* Corresponding author at: Reference Center for Neurometabolic Diseases, Department of Genetics, La Pitié-Salpêtrière University Hospital, 47 Boulevard de l'Hôpital, 75013 Paris, France.
E-mail address: fanny.mochel@upmc.fr (F. Mochel).
[1] These authors worked equally.

https://doi.org/10.1016/j.nicl.2021.102566
Received 28 October 2020; Received in revised form 31 December 2020; Accepted 11 January 2021
Available online 19 January 2021

1. Introduction

X-linked adrenoleukodystrophy is the most common peroxisomal disorder caused by mutations in the *ABCD1* gene that encodes ALDP, a peroxisomal membrane transporter. In the brain, ALDP is mainly expressed in astrocytes, microglia and endothelial cells. Pathogenic *ABCD1* variants impair peroxisomal beta-oxidation and lead to accumulation of very-long chain fatty acids (VLCFA) in various tissues including the brain, spinal cord, and the adrenal cortex (Aubourg et al., 1993; Mosser et al., 1993). Clinical phenotype varies according to age of onset and sex. Patients with adult-onset disease usually develop a clinically disabling myeloneuropathy with adrenal insufficiency (Adrenomyeloneuropathy: AMN). Male patients are more severely affected whereas female carriers present with less severe symptoms in adulthood (Engelen et al., 2014). Importantly, men are at-risk of demyelinating and inflammatory lesions of the brain. Annual brain imaging is warranted (or before, if new cerebral symptoms emerge) as disease may be halted with early hematopoietic stem cell transplantation (Raymond et al., 2019). While disease-modifying drugs (Marchetti et al., 2018; Casasnovas et al., 2019) and gene therapy (Eichler et al., 2017) are under evaluation for the myelopathy, at present symptomatic treatment only exists. Future disease modifying interventions will require accurate assessment of disease progression. In this regard, existing clinical scales are inadequate. A study with 25 AMN male patients demonstrated significant deterioration in the Expanded Disability Status Score (EDSS) and the Severity Scoring system for Progressive Myelopathy (SSPROM) over two years (Huffnagel et al., 2019a). However, effect sizes were small (Huffnagel et al., 2019a). This suggests clinical trials require longer follow-up and a large number of patients. Quantitative imaging biomarkers have been proposed as more sensitive outcome measures for assessing disease progression and therapeutic interventions (Castellano et al., 2016; Huffnagel et al., 2019b; Politi et al., 2019; van de Stadt et al., 2020).

AMN is principally a disease of the spinal cord (Powers et al., 2000); however, most imaging studies focus on the brain (Izquierdo et al., 2000; Dubey et al., 2005a, 2005b; Zackowski et al., 2006; Marino et al., 2007; Teriitehau et al., 2007; Ratai et al., 2008). To date, few studies evaluate both brain and spinal cord (Castellano et al., 2016; Huffnagel et al., 2019b; Politi et al., 2019; van de Stadt et al., 2020). This may be due to spine-specific imaging challenges such as strong susceptibility changes, physiological motion, inhomogeneity of the magnetic field and low signal-to-noise ratio (SNR) (Stroman et al., 2014). Therefore, improved acquisition techniques and analysis procedures are needed that overcome these limitations to effectively determine how AMN affects spine structure, microstructure and metabolism.

In this study, we used standardized acquisition techniques to evaluate the structural and microstructural alterations in the spine and brain of patients with AMN. Furthermore, we used advanced diffusion imaging analysis to evaluate the contribution of fiber density and fiber cross-section to the microstructural alterations. Finally, we used an improved and advanced magnetic resonance spectroscopy (MRS) techniques to elucidate the metabolic alterations in the spine of patients with AMN.

2. Methods

The local ethics committee approved the study (EudraCT 2017-000748-16). All participants were over 18 years and signed a written informed consent before they participated in the study.

2.1. Study participants

Twenty-three male patients with AMN (mean age: 44 ± 11) and 23 age- and sex-matched healthy controls (mean age: 43 ± 11) with no history of neurological issues were recruited for this study (Table 1) at the Brain and Spine Institute, Paris, France. Participants who were not able to undergo MRI, had inflammatory cerebral lesions or could not consent to the study protocol were excluded from the study. Disease severity in AMN patients was scored using the EDSS and the SSPROM.

Table 1
Demographic information on recruited participants.

	Controls	Patients	p value
Number of subjects	23	23	–
Gender	Male	Male	–
Age (years)	43 ± 11 [25–60]	44 ± 11 [23–59]	0.915
Body mass index (kg/m^2)	23.67 ± 2.92 [19.24–30.86]	24.97 ± 3.96 [19.44–35.44]	0.212
EDSS	–	4.59 ± 1.14 [2.5–6.0]	–
SSPROM	–	80.50 ± 4.53 [71.0–90.5]	–
Disease duration (years)	–	11 ± 7 [3–30]	–

Data are presented as mean ± standard deviation [range]. EDSS: Expanded disability status scale. SSPROM: Severity score system for progressive myelopathy. P values were calculated with Welch ANOVA.

2.2. Imaging protocol

MRI and MRS acquisitions were performed on a 3-Tesla Siemens Prisma fit scanner (Siemens Medical Solutions, Erlangen, Germany) using a standard Siemens body coil for transmit and a 64-channel head-neck coil together with a 32-channel spine coil for receive. A pulse oximeter was placed on the index finger for physiological monitoring and triggering of the spine diffusion sequences.

2.2.1. Spine imaging

We used a standardized consensus acquisition protocol of spinal cord imaging (Alley et al., 2018) to evaluate macrostructural and microstructural alterations in the spine. 3D *T2*-weighted spine images (T_R = 1500 ms, T_E = 120 ms, flip angle = 120°, voxel size = 0.8 mm isotropic, field of view (FOV) = 256 × 256 mm^2) were acquired for volumetric assessment. Axial *T2** multi-echo gradient-echo images (T_R = 600 ms, T_E = 14 ms, Combined echoes = 3, flip angle = 30°, voxel size = 0.5 × 0.5 × 5.0 mm, FOV = 224 × 224 mm^2) were acquired to segment the gray and white matter of the spinal cord. Furthermore, axial images without and with magnetization transfer at (T_R = 35 ms, T_E = 3.13 ms, flip angle = 9°, voxel size = 0.9 × 0.9 × 5.0 mm, FOV = 230 × 230 mm^2) were acquired at the C1-C5 levels to characterize the local cord environment. In addition, diffusion sensitizing encoding gradients were applied in 30 directions (T_R = 610 ms, T_E = 60 ms, flip angle = 90°, voxel size = 0.9 × 0.9 × 5.0 mm, FOV = 86 × 32 mm^2, *b* value = 800 s/mm^2), interleaved with 5 non-diffusion-weighted reference images (b0 images, *b* value = 0 s/mm^2). The diffusion acquisition was repeated with the opposite phase-encode scheme for distortion correction.

MRS was performed at the C3-C4 vertebral level using a modified version of the validated semi-LASER sequence (T_R = 5000 ms, T_E = 28 ms, averages = 128) (Oz and Tkac, 2011; Deelchand et al., 2015). A 30 ms asymmetric adiabatic radiofrequency pulse (Hwang et al., 1999) was added just before the semi-LASER sequence to selectively invert metabolites every other shot while the amplitude and phase of water remained untouched (Hock et al., 2013). Shimming was achieved with fast automatic shimming technique with echo-planar signal trains utilizing mapping along projections (Gruetter and Tkac, 2000). Unlike conventional MRS, the variable pulse power and optimized relaxation delays (VAPOR) water suppression pulses were calibrated to suppress the water signal only partially, retaining sufficient water peak SNR for shot-to-shot frequency correction. The power for the 90° asymmetric radiofrequency pulse as well as the outer volume suppression (OVS) pulses were calibrated in each subject. As previously described, two unsuppressed water spectra (2 averages each) were acquired: one for eddy current correction (the radiofrequency pulses of the VAPOR

scheme were turned off) and one for use as reference for metabolite quantification (radiofrequency pulses of both VAPOR and OVS schemes turned off in order to eliminate magnetization transfer effects) (Adanyeguh et al., 2015; Deelchand et al., 2015).

2.2.2. Brain imaging

A 3D *T1*-weighted magnetization-prepared rapid gradient-echo (MPRAGE) volumetric image (T_R = 2300 ms, T_E = 4.18 ms, T_I = 900 ms, flip angle = 9°, voxel size = 1 mm isotropic, FOV = 256 × 240 mm^2) was acquired for localization. An echo-planar spin-echo sequence was used to acquire diffusion data along 60 directions (T_R = 3500 ms, T_E = 75 ms, voxel size = 1.8 mm isotropic, FOV = 220 × 220 mm^2, multiband acceleration factor = 3, *b* value = 2000 s/mm^2), interleaved with 5 b0 images. The diffusion acquisition was repeated with the opposite phase-encode scheme for distortion correction. Axial *T1*-weighted (T_R = 8.6 ms, T_E = 4.0 ms, flip angle = 20°, voxel size = 0.5 × 0.5 × 7.0 mm, FOV = 250 × 250 mm^2) images with gadolinium contrast were acquired to evaluate the cerebral involvement of patients and their inclusion in the study.

2.3. Data analysis

2.3.1. Spinal cord morphometry

Quantitative image analysis was performed with the Spinal Cord Toolbox (SCT, version 4.0.0) (De Leener et al., 2017). The cord was segmented on the *T2*-weighted images with a deep learning segmentation algorithm in SCT. The C2-C3 intervertebral disc was manually labeled to improve the detection of the vertebral levels. The cord was straightened by following the automatically detected centerline. A combination of affine and non-linear symmetric transformations were used to finely match the PAM50 template (De Leener et al., 2018) to the *T2*-weighted image, while preserving the inner geometry of the cord (De Leener et al., 2017). The cross-sectional area (CSA) was then computed to cover the C1 to T2 vertebral levels.

Multi-echo *T2** images showed distinct gray/white matter contrast in controls but less so in AMN patients, likely due to neurodegeneration (Supplementary Fig. 1). Segmentation of the gray matter was therefore achieved with deep dilatated convolutions on the *T2**-weighted images. This deep learning algorithm improves gray matter segmentation in images where gray matter appears faint and manual segmentation fails (Perone et al., 2018).

2.3.2. Spinal cord magnetization transfer ratio (MTR)

Images with and without magnetization transfer contrast were rigidly co-registered to improve the estimation of MTR. The PAM50 template was registered to these images using the warping fields previously estimated from the spinal cord CSA analysis. This was achieved through slice-wise center of mass alignment and non-linear symmetric normalization regularized with b-splines (De Leener et al., 2017). MTR was then calculated as:

$$MTR = 1 - \frac{S_{MT1}}{S_{MT0}}$$

where S_{MT1} is the signal from the image with magnetization transfer applied, and S_{MT0} is the signal from the image without magnetization transfer.

MTR was estimated for vertebral levels C1-C5 and also specifically from the gray matter and 3 major white matter regions (dorsal columns, lateral funiculi and ventral funiculi) using the initial warping fields estimated from the segmentation of the *T2**-weighted images.

2.3.3. Metabolite quantification

Low SNR in spine MRS (due to the small size of the voxel) hinders shot-to-shot frequency and phase correction before summation. The data from this study however benefited from the high-water peak that allowed shot-to-shot frequency and phase corrections (Supplementary Fig. 2). By subtracting the alternating shots, the water signal was subtracted while the metabolite peaks added up (Supplementary Fig. 2). The spectra were corrected for eddy-current distortions using the unsuppressed water signal. Quantification of the metabolites were performed in the frequency domain using LCModel (Provencher, 1993) with a stimulated basis-set that was generated based on density matrix formalism (Deelchand et al., 2012). The concentrations of metabolites were obtained using water as an internal concentration reference. Only the four prominent metabolites myo-Ins, total choline (tCho, PCho + GPC), total creatine (tCr, Cr + PCr) and total NAA (tNAA, NAA + NAAG) were reported due to the high variability in the low concentration metabolites evident in the high Cramér-Rao lower bounds (CRLB), estimated errors of metabolite quantification.

2.3.4. Diffusion image analysis

The initial preprocessing of the brain and spine diffusion images were similar and utilized the MRtrix3 and FSL software packages. The data were processed to remove noise using principal component analysis based on the Marchenko-Pastur distribution (Veraart et al., 2016) and Gibbs-ringing artifacts were based on local sub-voxel shifts (Kellner et al., 2016). The data were then corrected for eddy currents, motion artifacts, susceptibility-induced off-resonance field distortions and bias due to B1 field inhomogeneity.

2.3.4.1. Diffusion tensor imaging (DTI). The corrected diffusion data were fitted to the diffusion tensor model to extract DTI metrics that include the fractional anisotropy (FA, describes the diffusion anisotropy), radial diffusivity (RD, describes diffusion perpendicular to the axons and can signal demyelination), axial diffusivity (AD, represents the main axis of diffusion) and mean diffusivity (MD, the average diffusion within a voxel). The PAM50 template was registered to the corrected spine DTI data using the warping fields that were estimated previously in order to extract the DTI metrics at the cervical levels C1-C5 and more specifically in the gray matter and the 3 major white matter regions. Brain DTI metrics were analyzed voxel-wise using Tract-based spatial statistics (TBSS) with threshold-free cluster enhancement (Smith et al., 2006).

2.3.4.2. Fiber tracking: Fixel-based analysis (FBA). The limitations associated with the DTI model inability to differentiate crossing-fibers (Alexander et al., 2002), and the stochastic and deterministic errors generated when used for fiber tracking (Jones et al., 2013) suggests the need for more advanced models that overcome these shortcomings. We performed FBA that uses probabilistic tractography to properly evaluate each fiber population (fixel) in a voxel as well as extract biologically meaningful metrics that can attribute changes to the fiber density (FD, number of axons), fiber cross-section (FC, total area occupied by axons) or a combination of fiber density and cross-section (FDC) (Raffelt et al., 2017).

The gray matter, white matter and cerebrospinal fluid (CSF) response functions from the bias corrected data were used to estimate the fiber orientation distribution (FOD) in the spine while only the white matter and CSF response functions were used to estimate the FOD in the brain using constrained spherical deconvolution (Dhollander et al., 2016). A single template FOD was generated from 8 patients and 8 controls to which each subject's FOD was registered. The FODs were then segmented to extract the metrics FD, FC and FDC (Raffelt et al., 2017).

2.4. Statistical analysis

Statistical analyses were performed using the R statistical software version 3.6.0 and the step-down Holm-Bonferroni correction was used to correct for multiple comparison. Demographic parameters including age and body-max index were compared using Welch ANOVA. Structural

and metabolic parameters from the spine were compared using Analysis of Covariance with age as a covariate. FSL randomize with 5000 permutations was used for voxel-wise comparisons of DTI metrics between patients and controls. The connectivity-based fixel enhancement (CFE) (Raffelt et al., 2015) was used to evaluate the FBA metrics between patients and controls. The CFE approach identifies fixels that are structurally connected using a whole-brain template tractogram generated from the template FOD. In doing so, tract-specific fixels are selected and analyzed and overcomes the problem of using multiple inclusion and exclusion masks to identify related tracts. Spearman correlation coefficients were calculated between imaging metrics and the clinical measures (EDSS, SSPROM and disease duration).

Furthermore, the effect sizes of metrics extracted from the spine, the primary site affected in AMN, was calculated in the patients compared to controls using the Cohen's *d* (Cohen, 1988) with the scale 0.2, 0.5, 0.8, 1.2 and 2.0 representing small, medium, large, very large and huge changes respectively (Cohen, 1988; Sawilowsky, 2009).

3. Results

3.1. Spine macrostructural alterations

Patients with AMN showed an average 20.9% reduction in the spine CSA compared to controls ($p < 0.001$). Atrophy was observed at all vertebral levels examined, C2-T2 ($p < 0.001$) (Fig. 1A). Though the absolute difference in CSA between patients and controls was higher in C1-C3 (17 mm^2) compared to T1-T2 (11 mm^2), the percent reduction in the cord CSA was higher in the thoracic levels, T1-T2 (25% reduction). The gray matter CSA was reduced by 28% ($p < 0.001$) while the white matter showed a 2% trend to decrease (Fig. 1B). Correlation was observed between EDSS and CSA at cervical levels C1_C2 (Spearman's rho = -0.506, p = 0.014), C3 (Spearman's rho = −0.430, p = 0.041), C5 (Spearman's rho = −0.441, p = 0.035) and C6 (Spearman's rho = −0.415, p = 0.049). Furthermore, correlation was observed between disease duration and CSA at cervical levels C1_C2 (Spearman's rho = −0.431, p = 0.045), C5 (Spearman's rho = −0.557, p = 0.007), C6 (Spearman's rho = −0.438, p = 0.042), and C8 (Spearman's rho = −0.468, p = 0.028).

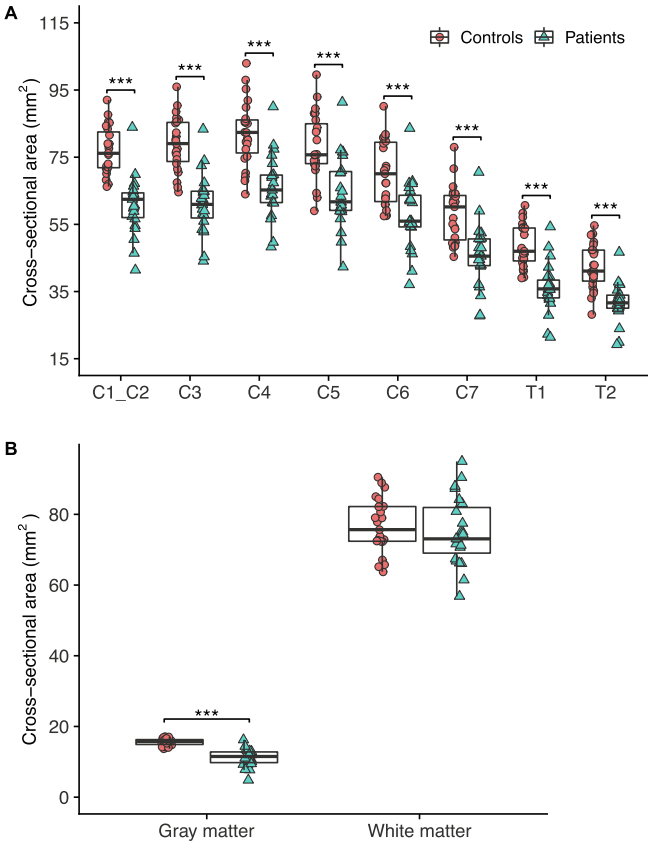

Fig. 1. Cross-sectional area of the spinal cord. Spine CSA was reduced in all vertebral regions in patients with AMN (A), and the decrease was more evident in the gray matter (B). (*** $p < 0.001$).

3.2. Spine metabolic alterations

The partially suppressed water peak allowed reliable shot-to-shot frequency and phase correction (Supplementary Fig. 2A), preventing loss of signal and broadening of linewidth during averaging. The four main peaks of tNAA, myo-Ins, tCr and tCho were readily apparent in the spine spectra (Supplementary Fig. 2C). Absolute concentrations showed an increasing trend in myo-Ins of patients relative to controls ($p = 0.07$) while tNAA significantly decreased ($p < 0.001$) (Fig. 2A). The ratio of tNAA/*myo*-Ins also significantly decreased in patients ($p < 0.001$) (Fig. 2B).

3.3. Spine microstructural alterations

MTR was reduced in cervical vertebrae C1 to C5 by 6.7% in gray matter and 10.6% in white matter of the spine ($p < 0.001$). The MTR was reduced at all cervical vertebral levels examined, C1-C5 ($p < 0.001$) (Fig. 3A) and more specifically in the gray matter and the 3 major white matter regions – dorsal columns, lateral and ventral funiculi ($p < 0.001$) (Fig. 3B). FA was significantly reduced in C3-C5 of patients ($p < 0.001$) and showed a trend to decrease in C1-C2 ($p = 0.160$) (Fig. 4A). There was more variability at C1-C2, likely due to higher B_0 inhomogeneity at

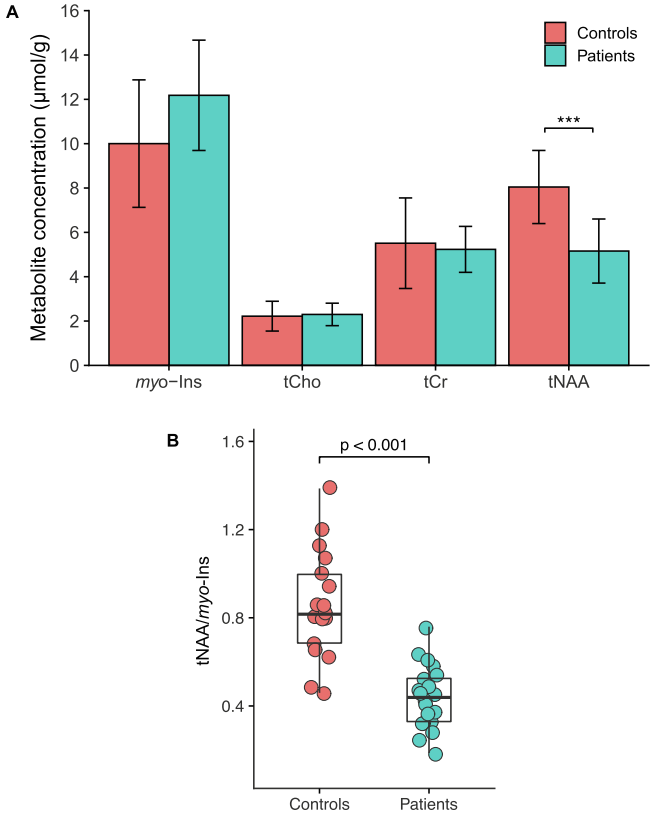

Fig. 2. Metabolite alterations in the spinal cord. Absolute concentrations showed a significantly reduced tNAA and a trend to increase in *myo*-Ins in patients with AMN (A). The ratio of tNAA/*myo*-Ins was significantly decreased in patients compared to controls (B). tNAA, total *N*-acetylaspartate; tCr, total creatine; tCho, total choline; *myo*-Ins, myo-Inositol. (*** $p < 0.001$).

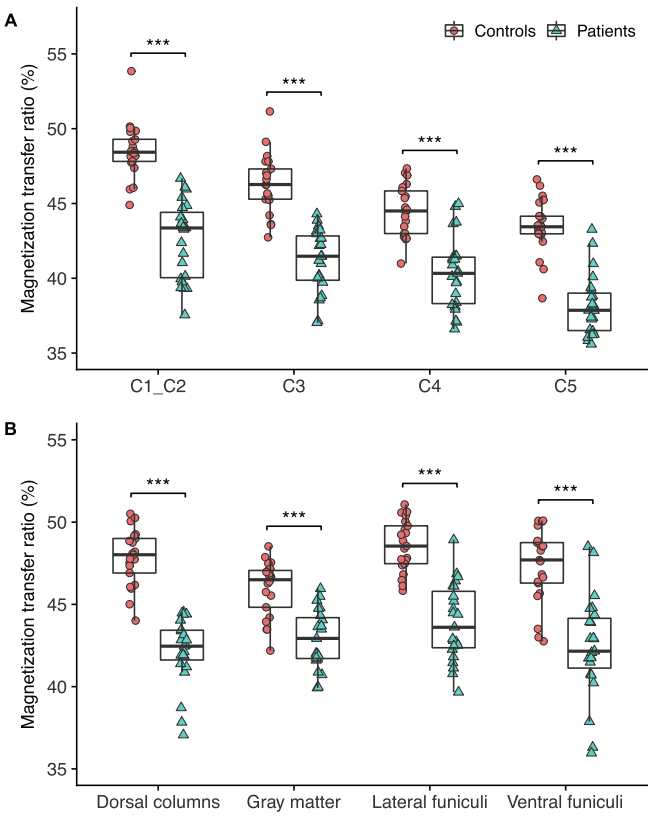

Fig. 3. Percentage MTR changes in the spinal cord. MTR was markedly reduced in cervical levels C1-C5 in patients with AMN (A) and in the spine gray matter and white matter regions examined (B). (*** $p < 0.001$).

the edge of the FOV. More specifically, FA significantly decreased in the gray matter, dorsal columns, the lateral and ventral funiculi ($p < 0.001$) (Fig. 4B). There was an overall 18% decrease in FA in patients with AMN. RD showed a significant increase only in the ventral funiculi (0.00060 mm^2/s in patients and 0.00047 mm^2/s in controls; $p < 0.001$) while there was no change in AD and MD. At the vertebral level, RD and MD showed a trend to increase in C3-C5 while AD showed a trend to decrease in C1-C5 in patients compared to controls (Supplementary Fig. 3). FBA on the other hand revealed a significant decrease in the FD, FC and FDC ($p < 0.001$) (Fig. 4C). Thus, we observed a 23% decrease in fiber density (FD), 17% decrease in the fiber bundle cross-section (FC) that signify atrophy of the fiber bundles and 22% decrease in the combined measure of the FD and FC (FDC) in patients with AMN. FA in the ventral funiculi correlated with EDSS (Spearman's rho = -0.434, p = 0.038) and SSPROM (Spearman's rho = 0.518, p = 0.014). Furthermore, SSPROM correlated with FA in the lateral funiculi (Spearman's rho = 0.426, p = 0.048) and cervical level C4 (Spearman's rho = 0.512, p = 0.015). In addition, FC correlated with SSPROM (Spearman's rho = 0.425, p = 0.049).

3.4. Effect size of spine imaging metrics

The imaging metrics used to probe the spinal cord in the cohort of patients with AMN had very large effect size with the exception of RD. Overall, MTR showed the largest effect size (Fig. 5).

3.5. Brain microstructural alterations

TBSS revealed decreased FA in several brain white matter regions including the corticospinal tract, internal capsule, external capsule, corpus callosum, cerebellar peduncles, corona radiata and longitudinal fasciculus compared to controls ($p < 0.05$) and this was associated with

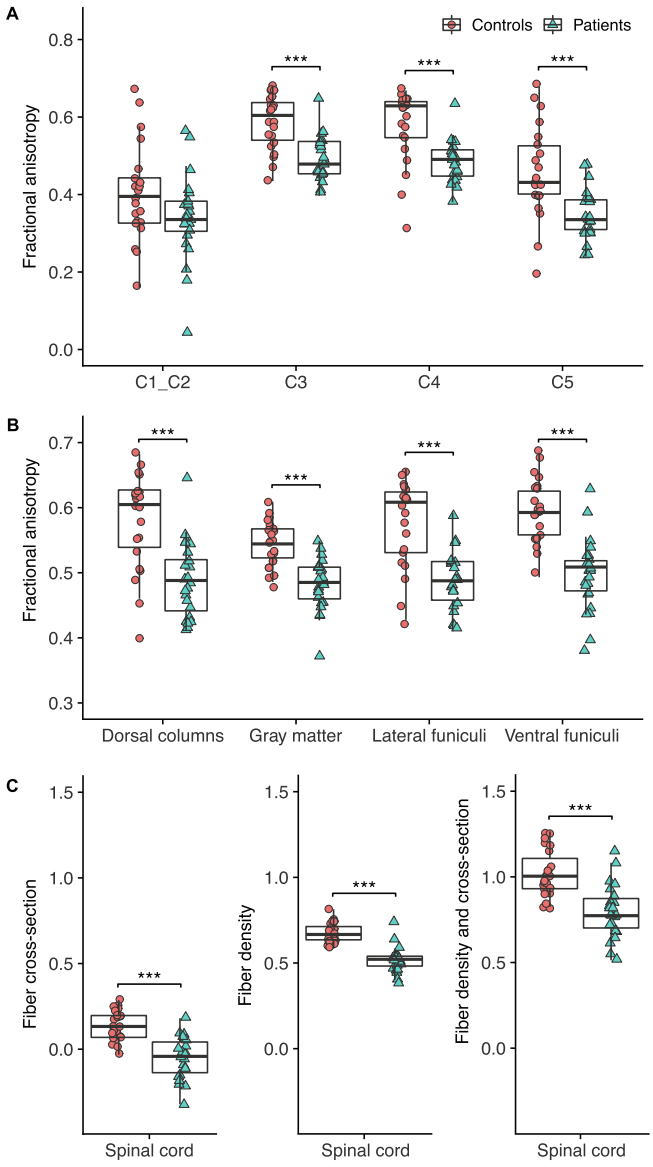

Fig. 4. Alterations in DTI and FBA metrics in the spinal cord. FA was reduced in C3-C5 in patients (A), and in the gray matter and white mater regions examined (B). FC, FD and FDC were reduced in the spine of patients compared to controls (C). FC values have been log normalized for normal distribution and to center the mean around zero. FC, fiber cross-section; FD, fiber density; FDC, fiber density and cross-section. (*** $p < 0.001$).

increased MD, RD and AD ($p < 0.05$) (Fig. 6A). FBA showed decreased FD, FC and FDC in the lower corticospinal tract (CST) ($p < 0.05$). FD and FDC were also significantly reduced in the corpus callosum, internal capsule and corona radiata ($p < 0.05$) (Fig. 6B).

4. Discussion

The novelty from this study lies in its fine characterization of the structure, microstructure and metabolism of the spine from AMN male patients compared to controls.

First, our study provides the first characterization of metabolic alterations in the spine of men with AMN using spinal cord MRS. Previous metabolic studies in AMN have been limited to the brain (Izquierdo et al., 2000; Dubey et al., 2005a; Marino et al., 2007; Teriitehau et al., 2007; Ratai et al., 2008) due to the challenges associated with spine MRS – susceptibility induced magnetic field inhomogeneities, low SNR, phase and frequency fluctuations resulting from physiological motion and

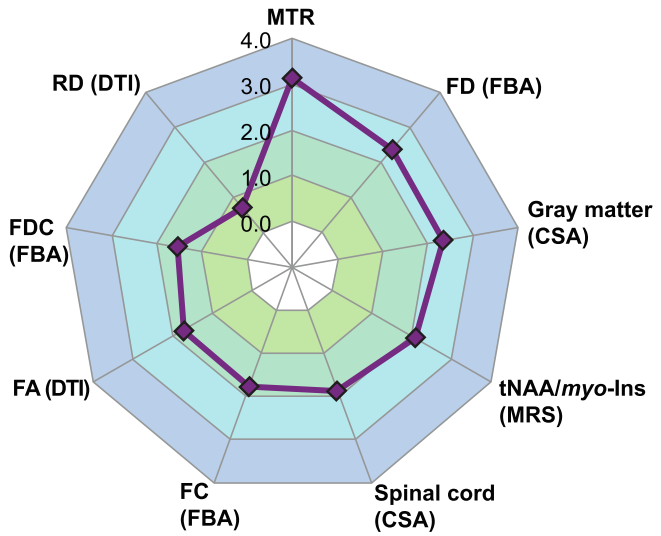

Fig. 5. Effect sizes of spinal cord imaging metrics. The spinal cord imaging metrics showed very large to huge effect sizes with the exception of RD that showed a very small effect size. MTR showed the largest effect size among all the metrics. MTR, magnetization transfer ratio; FD, fiber density; FBA, fixel-based analysis; CSA, cross-sectional area; tNAA, total *N*-acetylaspartate; *myo*-Ins, myo-Inositol; MRS, magnetic resonance spectroscopy; FC, fiber cross-section; FA, fractional anisotropy; DTI, diffusion tensor imaging; FDC, fiber density and cross-section; RD, radial diffusivity.

respiration as well as lipid contamination (Gomez-Anson et al., 2000; Cooke et al., 2004). Here, we used a validated semi-LASER sequence with low chemical-shift displacement error (Deelchand et al., 2015), a pulse-oximeter to limit motion artifacts due to physiological motion, OVS to reduce lipid contamination, and metabolite-cycling allowing shot-to-shot frequency and phase correction from the partially suppressed water peak. The absolute concentrations showed high inter-subject variability, presumably due to variable amounts of CSF in the voxel; hence, we reported the ratio of two metabolites, *myo*-Ins (i.e. a glial marker) and tNAA (i.e. a neuronal marker). Our data suggest a neuronal-glial impairment in AMN spinal pathology. ALDP is expressed in microglia cells and histopathological studies have identified activated microglia in the spine of AMN patients (Powers et al., 2000). Our findings of increased glial marker, *myo*-Ins, in patients with AMN could therefore point to a contribution of microglial cells to the pathology. The large effect size of tNAA/*myo*-Ins ratio may be particularly suitable as a surrogate biomarker to evaluate metabolic therapies in AMN.

Second, our findings of decreased spine CSA from C1-T2 agrees with three previous studies (Castellano et al., 2016; Politi et al., 2019; van de Stadt et al., 2020). This reduction in spine CSA can be attributed to spinal tract degeneration in AMN (Powers, 1995). We studied the proportional contribution of gray and white matter and identified significant gray matter atrophy in our patient cohort. To further characterize the cord environment, we reported reduced MTR at all cord levels, as well as in the gray matter and white mater of patients with AMN. Magnetization transfer is a technique that preferentially saturates macromolecule-bound protons and then measures the transfer of magnetization to the free mobile or liquid protons (Henkelman et al., 2001). The exchange of magnetization allows the quantification of the macromolecule-bound protons which otherwise could not be measured directly due to their very short *T2* (Henkelman et al., 2001). Reduced MTR has been linked to demyelination or reduced myelin content in multiple sclerosis (Schmierer et al., 2004; McCreary et al., 2009), a disease associated with axonal demyelination. Powers et al. reported that axonal loss is equal to or greater than myelin loss in *post-mortem* specimen from 5 AMN/ALD patients (Powers et al., 2000). The reduced MTR in our cohort could therefore be as a result of reduced number and size of axons or reduced myelin content in the spine of patients with AMN. Of all imaging metrics, MTR demonstrated the largest effect size highlighting its specificity for delineating the cord environment. Moreover, while the gray matter was previously thought to be unremarkable in 10 *post-mortem* AMN/ALD patients (Powers et al., 2000), our *in vivo* findings in 23 AMN patients suggest gray matter involvement in the pathology. The increased gray matter atrophy and the reduced gray matter MTR could point to neuronal loss in the gray matter as well as decreased myelination in the gray matter. Nonetheless, in order to use these spinal cord characterization techniques in clinical trials, the quantification methods must be more robust with negligible experimenter bias in their implementation. In a previous study in spinocerebellar ataxia (Adanyeguh et al., 2018) we showed that automated methods are more sensitive to detect longitudinal changes and less time consuming compared to methods that relied a lot on manual approaches. Thus, the combination of these macro- and microstructural metrics with deep learning approaches (De Leener et al., 2017) may be more suitable for clinical trials.

Third, our diffusion tensor analysis in the spinal cord revealed microstructural alterations in the form of reduced FA at C3-C5, in agreement with previous studies (Castellano et al., 2016; Huffnagel et al., 2019b; Politi et al., 2019). However, in contrast to these studies, we observed no significant change in AD and RD at any cervical level, except for a small increase in RD specifically in the ventral funiculi. Similar to (Castellano et al., 2016) but unlike (Huffnagel et al., 2019b), we observed no significant change in MD at any cervical levels. These differences may result from a lack of effective correction of susceptibility induced distortions (common in the spinal cord) in previous studies. Unlike the reversed phase-encode method of distortion correction in this study, lack of susceptibility distortion correction (Castellano et al., 2016) and use of susceptibility distortion correction based on anatomical co-registration (Huffnagel et al., 2019b) have been shown to negatively impact DTI metric estimation and fiber tracking in the spine (Cohen-Adad et al., 2009). Furthermore, the lack of significant increase in RD, a metric of demyelination, at all cervical levels suggests that axonal loss may be greater than myelin loss in our cohort. Findings from a previous study (Huffnagel et al., 2019b) also favors axonal degeneration in the spine. While DTI metrics are easy to extract in a clinical setting, their biological interpretation can sometimes be quite ambiguous and non-specific (Jones et al., 2013). Accordingly, we used fiber tracking to estimate the number of axons and the space they occupy in order to elucidate the specific spine microstructural changes occurring in AMN. Likewise, we were able to directly attribute spine microstructural changes to reduced number of axons (FD), atrophy of the axons which could result from demyelination or hypomyelination (FC) and a combination of both metrics (FDC).

In the brain, we observed microstructural alterations in several brain regions including the corticospinal tract, internal and external capsules, corpus callosum, longitudinal fasciculus, anterior thalamic radiation, cingulum and cerebellar peduncles. Similar changes have been reported (Castellano et al., 2016), although with a very low number of diffusion directions (6 directions). In the present study, decreased FA was associated with increased RD and MD, and AD was also increased in a few brain white matter regions. These findings suggest possible demyelination in the brain, with a possible loss of neurons and changes to the neuronal cytoskeleton and viscosity. However, the DTI assumption that each voxel contains only one fiber is untrue as it has been shown that as much as 93% of white matter voxels contain multiple crossing fibers (Jeurissen et al., 2013). There is thus a need for fiber tracking to define fiber pathways. Using fiber tracking in the brain of patients with AMN, reduced neuronal fibers have been reported in the CST (Dubey et al., 2005b), as well as decreased FA and increased RD and MD in the lower parts of the CST (Castellano et al., 2016; Huffnagel et al., 2019b). Still, these studies failed to extract quantitative measures that provide specific explanations for the observed changes. Furthermore, the use of manual delineation of regions of interest (Huffnagel et al., 2019b) is prone to

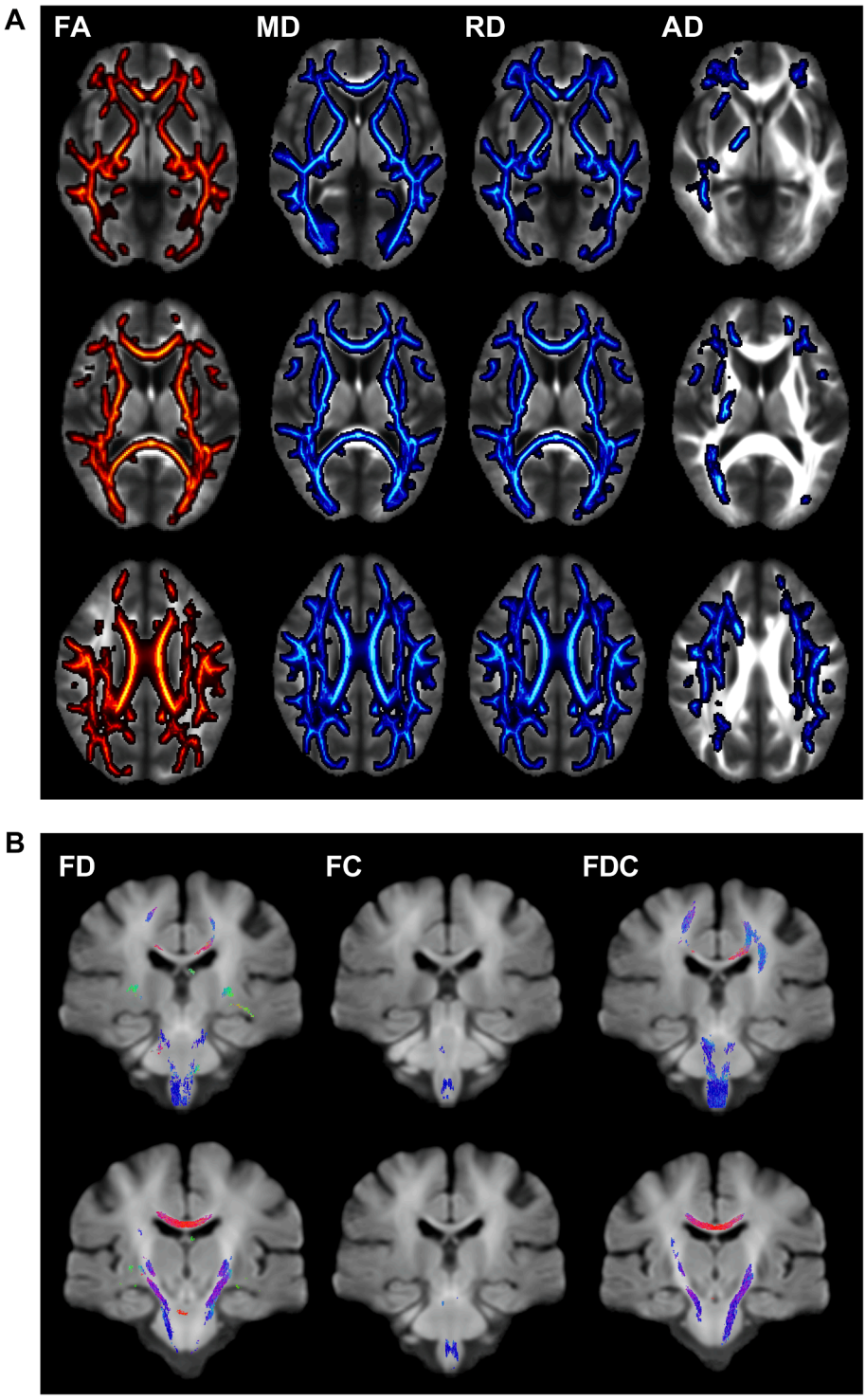

Fig. 6. Brain microstructural alterations between patients and controls. DTI metrics showed significantly increased FA and reduced MD, RD and AD in the brain of patients with AMN compared to controls (A). FBA metrics showed significantly reduced fixel in the corticospinal tract and corpus callosum of patients with AMN compared to controls (B). FA, fractional anisotropy; MD, mean diffusivity; RD, radial diffusivity; AD, axial diffusivity; FD, fiber density; FC, fiber cross-section; FDC, fiber density and cross-section.

experimenter bias. By incorporating FBA in our study, we removed the problem of experimenter bias. Considering the overlap in microstructural changes we observed with DTI and FBA metrics, it seems that both metrics complement each other. However, the limitations of DTI in terms of averaging of voxels that contain crossing-fibers constraints their biological interpretation. Hence, FBA metrics with their anatomical specificity are more likely to provide meaningful biological interpretation. FD is proportional to the intra-axonal volume (Raffelt et al., 2017) and thus a decrease in FD in patients with AMN specifically points to a decrease in the fiber bundle. FD thus provides us with information pertaining to the microstructural changes in the neuronal fibers. FC on the other hand relates to the changes in the size of the fiber bundle cross-section (Raffelt et al., 2017) and thus reflects the macrostructural changes due to atrophy, that could result from demyelination or hypomyelination. By combining these two metrics, we could identify tracts that were altered as a result of reduction in the number and cross-sectional size of the fibers. The ability to attribute changes in FBA metrics to specific biological alterations make the FBA method especially suitable for clinical trials.

In conclusion, our study contributes to the accurate delineation of

the structural, microstructural and metabolic alterations that occur in the spine and the brain of AMN men. The high effect size of these quantitative neuroimaging metrics, especially in the spinal cord, makes them suitable candidates for surrogate outcome measures in AMN, and possibly other spinal cord disorders. To evaluate their performance over time, these outcome measures should be tested longitudinally and in clinical trials.

CRediT authorship contribution statement

Isaac M. Adanyeguh: Methodology, Software, Validation, Formal analysis, Investigation, Data curation, Visualization, Writing - original draft. **Xiaofang Lou:** Software, Validation, Formal analysis, Data curation, Visualization, Writing - review & editing. **Eavan McGovern:** Investigation, Supervision, Writing - review & editing. **Marie-Pierre Luton:** Supervision, Project administration, Writing - review & editing. **Magali Barbier:** Project administration, Writing - review & editing. **Elise Yazbeck:** Investigation, Supervision, Writing - review & editing. **Romain Valabregue:** Methodology, Writing - review & editing. **Dinesh Deelchand:** Methodology, Software, Writing - review & editing. **Pierre-Gilles Henry:** Methodology, Software, Writing - review & editing. **Fanny Mochel:** Conceptualization, Methodology, Validation, Resources, Supervision, Funding acquisition, Writing - review & editing.

Declaration of Competing Interest

The authors declare that they have no known competing financial interests or personal relationships that could have appeared to influence the work reported in this paper.

Acknowledgements

We are very grateful to the patients and volunteers who participated in this study. CMRR is supported by NIH grants P41EB027061 and P30NS076408.

Study funding

This study was sponsored and funded by Minoryx Therapeutics. This study was financially supported by the "Investissements d'avenir" program ANR-10-IAIHU-06 (IHU-A-ICM).

Full financial disclosure

No disclosure: Adanyeguh, Lou, McGovern, Luton, Barbier, Yazbeck, Valabregue, and Deelchand.

Dr Henry received research support from Minoryx Therapeutics, Friedreich's Ataxia Research Alliance (FARA), and NIH.

Dr Mochel received research support by grants from INSERM, the French Agency for Research, Carnot Institutes, ASL Foundation, Ultragenyx Pharmaceutical and Minoryx Therapeutics.

Appendix A. Supplementary data

Supplementary data to this article can be found online at https://doi.org/10.1016/j.nicl.2021.102566.

References

Adanyeguh, I.M., Henry, P.G., Nguyen, T.M., Rinaldi, D., Jauffret, C., Valabregue, R., Emir, U.E., Deelchand, D.K., Brice, A., Eberly, L.E., Oz, G., Durr, A., Mochel, F., 2015. In vivo neurometabolic profiling in patients with spinocerebellar Ataxia types 1, 2, 3, and 7. Mov. Disord. 30 (5), 662–670.

Adanyeguh, I.M., Perlbarg, V., Henry, P.G., Rinaldi, D., Petit, E., Valabregue, R., Brice, A., Durr, A., Mochel, F., 2018. Autosomal dominant cerebellar ataxias: Imaging biomarkers with high effect sizes. Neuroimage Clin. 19, 858–867.

Alexander, D.C., Barker, G.J., Arridge, S.R., 2002. Detection and modeling of non-Gaussian apparent diffusion coefficient profiles in human brain data. Magn. Reson. Med. 48 (2), 331–340.

Alley, S., Gilbert, G., Gandini, W.-K.,C.A., Samson, R., Grussu, F., Martin, A.R., Bannier, E., Callot, V., Smith, S.A., Xu, S., Dewey, B., Weber, K.A., Parrish, T.B., McLaren, D., Barker, G.J., Papinutto, N., Seif, M., Freund, P., Barry, R.L., By, S., Narayanan, S., Cohen-Adad, J., 2018. Consensus acquisition protocol for quantitative MRI of the cervical spinal cord at 3T. In: Paper presented at the 26th Annual Meeting of ISMRM, Paris.

Aubourg, P., Mosser, J., Douar, A.M., Sarde, C.O., Lopez, J., Mandel, J.L., 1993. Adrenoleukodystrophy gene: unexpected homology to a protein involved in peroxisome biogenesis. Biochimie 75 (3–4), 293–302.

Casasnovas, C., Ruiz, M., Schlüter, A., Naudí, A., Fourcade, S., Veciana, M., Castañer, S., Albertí, A., Bargalló, N., Johnson, M., Raymond, G.V., Fatemi, A., Moser, A.B., Villarroya, F., Portero-Otín, M., Artuch, R., Pamplona, R., Pujol, A., 2019. Biomarker identification, safety, and efficacy of high-dose antioxidants for adrenomyeloneuropathy: a phase II pilot study. Neurotherapeutics 16 (4), 1167–1182.

Castellano, A., Papinutto, N., Cadioli, M., Brugnara, G., Iadanza, A., Scigliuolo, G., Pareyson, D., Uziel, G., Kohler, W., Aubourg, P., Falini, A., Henry, R.G., Politi, L.S., Salsano, E., 2016. Quantitative MRI of the spinal cord and brain in adrenomyeloneuropathy: in vivo assessment of structural changes. Brain 139 (Pt 6), 1735–1746.

Cohen, J., 1988. Statistical Power Analysis for the Behavioral Sciences, second ed. Lawrence Erlbaum Associates, USA.

Cohen-Adad, J., Lundell, H., Rossignol, S., 2009. Distortion correction in spinal cord DTI: What's the best approach? Proc. Intl. Soc. Mag. Reson. Med. 17, 3178.

Cooke, F.J., Blamire, A.M., Manners, D.N., Styles, P., Rajagopalan, B., 2004. Quantitative proton magnetic resonance spectroscopy of the cervical spinal cord. Magn. Reson. Med. 51 (6), 1122–1128.

De Leener, B., Fonov, V.S., Collins, D.L., Callot, V., Stikov, N., Cohen-Adad, J., 2018. PAM50: Unbiased multimodal template of the brainstem and spinal cord aligned with the ICBM152 space. Neuroimage 165, 170–179.

De Leener, B., Levy, S., Dupont, S.M., Fonov, V.S., Stikov, N., Louis Collins, D., Callot, V., Cohen-Adad, J., 2017. SCT: Spinal Cord Toolbox, an open-source software for processing spinal cord MRI data. Neuroimage 145 (Pt A), 24–43.

Deelchand, D.K., Adanyeguh, I.M., Emir, U.E., Nguyen, T.M., Valabregue, R., Henry, P. G., Mochel, F., Oz, G., 2015. Two-site reproducibility of cerebellar and brainstem neurochemical profiles with short-echo, single-voxel MRS at 3T. Magn. Reson. Med. 73 (5), 1718–1725.

Deelchand, D.K., Henry, P.G., Uğurbil, K., Marjańska, M., 2012. Measurement of transverse relaxation times of J-coupled metabolites in the human visual cortex at 4 T. Magn. Reson. Med. 67 (4), 891–897.

Dhollander, T., Raffelt, D., Connelly, A., 2016. Unsupervised 3-tissue response function estimation from single-shell or multi-shell diffusion MR data without a co-registered T1 image. In: ISMRM Workshop on Breaking the Barriers of Diffusion MRI, pp. 5.

Dubey, P., Fatemi, A., Barker, P.B., Degaonkar, M., Troeger, M., Zackowski, K., Bastian, A., Smith, S.A., Pomper, M.G., Moser, H.W., Raymond, G.V., 2005a. Spectroscopic evidence of cerebral axonopathy in patients with "pure" adrenomyeloneuropathy. Neurology 64 (2), 304–310.

Dubey, P., Fatemi, A., Huang, H., Nagae-Poetscher, L., Wakana, S., Barker, P.B., van Zijl, P., Moser, H.W., Mori, S., Raymond, G.V., 2005b. Diffusion tensor-based imaging reveals occult abnormalities in adrenomyeloneuropathy. Ann. Neurol. 58 (5), 758–766.

Eichler, F., Duncan, C., Musolino, P.L., Orchard, P.J., De Oliveira, S., Thrasher, A.J., Armant, M., Dansereau, C., Lund, T.C., Miller, W.P., Raymond, G.V., Sankar, R., Shah, A.J., Sevin, C., Gaspar, H.B., Gissen, P., Amartino, H., Bratkovic, D., Smith, N. J.C., Paker, A.M., Shamir, E., O'Meara, T., Davidson, D., Aubourg, P., Williams, D.A., 2017. Hematopoietic stem-cell gene therapy for cerebral adrenoleukodystrophy. N. Engl. J. Med. 377 (17), 1630–1638.

Engelen, M., Kemp, S., Poll-The, B.T., 2014. X-linked adrenoleukodystrophy: pathogenesis and treatment. Curr. Neurol. Neurosci. Rep. 14 (10), 486.

Gomez-Anson, B., MacManus, D.G., Parker, G.J., Davie, C.A., Barker, G.J., Moseley, I.F., McDonald, W.I., Miller, D.H., 2000. In vivo 1H-magnetic resonance spectroscopy of the spinal cord in humans. Neuroradiology 42 (7), 515–517.

Gruetter, R., Tkac, I., 2000. Field mapping without reference scan using asymmetric echo-planar techniques. Magn. Reson. Med. 43 (2), 319–323.

Henkelman, R.M., Stanisz, G.J., Graham, S.J., 2001. Magnetization transfer in MRI: a review. NMR Biomed. 14 (2), 57–64.

Hock, A., MacMillan, E.L., Fuchs, A., Kreis, R., Boesiger, P., Kollias, S.S., Henning, A., 2013. Non-water-suppressed proton MR spectroscopy improves spectral quality in the human spinal cord. Magn. Reson. Med. 69 (5), 1253–1260.

Huffnagel, I.C., van Ballegoij, W.J.C., van Geel, B.M., Vos, J., Kemp, S., Engelen, M., 2019a. Progression of myelopathy in males with adrenoleukodystrophy: towards clinical trial readiness. Brain 142 (2), 334–343.

Huffnagel, I.C., van Ballegoij, W.J.C., Vos, J., Kemp, S., Caan, M.W.A., Engelen, M., 2019b. Longitudinal diffusion MRI as surrogate outcome measure for myelopathy in adrenoleukodystrophy. Neurology 93 (23), e2133–e2143.

Hwang, T.L., van Zijl, P.C., Garwood, M., 1999. Asymmetric adiabatic pulses for NH selection. J. Magn. Reson. 138 (1), 173–177.

Izquierdo, M., Adamsbaum, C., Benosman, A., Aubourg, P., Bittoun, J., 2000. MR spectroscopic imaging of normal-appearing white matter in adrenoleukodystrophy. Pediatr. Radiol. 30 (9), 621–629.

Jeurissen, B., Leemans, A., Tournier, J.D., Jones, D.K., Sijbers, J., 2013. Investigating the prevalence of complex fiber configurations in white matter tissue with diffusion magnetic resonance imaging. Hum. Brain Mapp. 34 (11), 2747–2766.

Jones, D.K., Knosche, T.R., Turner, R., 2013. White matter integrity, fiber count, and other fallacies: the do's and don'ts of diffusion MRI. Neuroimage 73, 239–254.
Kellner, E., Dhital, B., Kiselev, V.G., Reisert, M., 2016. Gibbs-ringing artifact removal based on local subvoxel-shifts. Magn. Reson. Med. 76 (5), 1574–1581.
Marchetti, D.P., Steffens, L., Jacques, C.E., Guerreiro, G.B., Mescka, C.P., Deon, M., de Coelho, D.M., Moura, D.J., Viario, A.G., Poletto, F., Coitinho, A.S., Jardim, L.B., Vargas, C.R., 2018. Oxidative imbalance, nitrative stress, and inflammation in C6 glial cells exposed to hexacosanoic acid: protective effect of N-acetyl-L-cysteine, trolox, and rosuvastatin. Cell. Mol. Neurobiol. 38 (8), 1505–1516.
Marino, S., De Luca, M., Dotti, M.T., Stromillo, M.L., Formichi, P., Galluzzi, P., Mondelli, M., Bramanti, P., Federico, A., De Stefano, N., 2007. Prominent brain axonal damage and functional reorganization in "pure" adrenomyeloneuropathy. Neurology 69 (12), 1261–1269.
McCreary, C.R., Bjarnason, T.A., Skihar, V., Mitchell, J.R., Yong, V.W., Dunn, J.F., 2009. Multiexponential T2 and magnetization transfer MRI of demyelination and remyelination in murine spinal cord. Neuroimage 45 (4), 1173–1182.
Mosser, J., Douar, A.M., Sarde, C.O., Kioschis, P., Feil, R., Moser, H., Poustka, A.M., Mandel, J.L., Aubourg, P., 1993. Putative X-linked adrenoleukodystrophy gene shares unexpected homology with ABC transporters. Nature 361 (6414), 726–730.
Oz, G., Tkac, I., 2011. Short-echo, single-shot, full-intensity proton magnetic resonance spectroscopy for neurochemical profiling at 4 T: validation in the cerebellum and brainstem. Magn. Reson. Med. 65 (4), 901–910.
Perone, C.S., Calabrese, E., Cohen-Adad, J., 2018. Spinal cord gray matter segmentation using deep dilated convolutions. Sci. Rep. 8 (1), 5966.
Politi, L.S., Castellano, A., Papinutto, N., Mauro, E., Pareyson, D., Henry, R.G., Falini, A., Salsano, E., 2019. Longitudinal quantitative magnetic resonance imaging in adrenomyeloneuropathy. Eur. J. Neurol.
Powers, J.M., 1995. The pathology of peroxisomal disorders with pathogenetic considerations. J. Neuropathol. Exp. Neurol. 54 (5), 710–719.
Powers, J.M., DeCiero, D.P., Ito, M., Moser, A.B., Moser, H.W., 2000. Adrenomyeloneuropathy: a neuropathologic review featuring its noninflammatory myelopathy. J. Neuropathol. Exp. Neurol. 59 (2), 89–102.
Provencher, S.W., 1993. Estimation of metabolite concentrations from localized in vivo proton NMR spectra. Magn. Reson. Med. 30 (6), 672–679.
Raffelt, D.A., Smith, R.E., Ridgway, G.R., Tournier, J.D., Vaughan, D.N., Rose, S., Henderson, R., Connelly, A., 2015. Connectivity-based fixel enhancement: Whole-brain statistical analysis of diffusion MRI measures in the presence of crossing fibres. Neuroimage 117, 40–55.
Raffelt, D.A., Tournier, J.D., Smith, R.E., Vaughan, D.N., Jackson, G., Ridgway, G.R., Connelly, A., 2017. Investigating white matter fibre density and morphology using fixel-based analysis. Neuroimage 144 (Pt A), 58–73.
Ratai, E., Kok, T., Wiggins, C., Wiggins, G., Grant, E., Gagoski, B., O'Neill, G., Adalsteinsson, E., Eichler, F., 2008. Seven-Tesla proton magnetic resonance spectroscopic imaging in adult X-linked adrenoleukodystrophy. Arch. Neurol. 65 (11), 1488–1494.
Raymond, G.V., Aubourg, P., Paker, A., Escolar, M., Fischer, A., Blanche, S., Baruchel, A., Dalle, J.H., Michel, G., Prasad, V., Miller, W., Paadre, S., Balser, J., Kurtzberg, J., Nascene, D.R., Orchard, P.J., Lund, T., 2019. Survival and Functional Outcomes in Boys with Cerebral Adrenoleukodystrophy with and without Hematopoietic Stem Cell Transplantation. Biol. Blood Marrow Transpl. 25 (3), 538–548.
Sawilowsky, S., 2009. New effect size rules of thumb. J. Mod. Appl. Stat. Methods 8 (2), 467–474.
Schmierer, K., Scaravilli, F., Altmann, D.R., Barker, G.J., Miller, D.H., 2004. Magnetization transfer ratio and myelin in postmortem multiple sclerosis brain. Ann. Neurol. 56 (3), 407–415.
Smith, S.M., Jenkinson, M., Johansen-Berg, H., Rueckert, D., Nichols, T.E., Mackay, C.E., Watkins, K.E., Ciccarelli, O., Cader, M.Z., Matthews, P.M., Behrens, T.E., 2006. Tract-based spatial statistics: voxelwise analysis of multi-subject diffusion data. Neuroimage 31 (4), 1487–1505.
Stroman, P.W., Wheeler-Kingshott, C., Bacon, M., Schwab, J.M., Bosma, R., Brooks, J., Cadotte, D., Carlstedt, T., Ciccarelli, O., Cohen-Adad, J., Curt, A., Evangelou, N., Fehlings, M.G., Filippi, M., Kelley, B.J., Kollias, S., Mackay, A., Porro, C.A., Smith, S., Strittmatter, S.M., Summers, P., Tracey, I., 2014. The current state-of-the-art of spinal cord imaging: methods. Neuroimage 84, 1070–1081.
Teriitehau, C., Adamsbaum, C., Merzoug, V., Kalifa, G., Tourbah, A., Aubourg, P., 2007. Subtle brain abnormalities in adrenomyeloneuropathy. J. Radiol. 88 (7–8 Pt 1), 957–961.
van de Stadt, S.I.W., van Ballegoij, W.J.C., Labounek, R., Huffnagel, I.C., Kemp, S., Nestrasil, I., Engelen, M., 2020. Spinal cord atrophy as a measure of severity of myelopathy in adrenoleukodystrophy. J. Inherit. Metab. Dis.
Veraart, J., Novikov, D.S., Christiaens, D., Ades-Aron, B., Sijbers, J., Fieremans, E., 2016. Denoising of diffusion MRI using random matrix theory. Neuroimage 142, 394–406.
Zackowski, K.M., Dubey, P., Raymond, G.V., Mori, S., Bastian, A.J., Moser, H.W., 2006. Sensorimotor function and axonal integrity in adrenomyeloneuropathy. Arch. Neurol. 63 (1), 74–80.